Supporting Information

Balancing Moisture and Oxygen Can Match the Crystallization Dynamics of Inert Halide Perovskite Processing

Maimur Hossain[1], Connor J. Dolan[1], Eric Oberholtz[1], Darya Kamiyama[1], Jack R. Palmer[2], Paulo E. Marchezi[1], Tim Kodalle[3,4], Carolin M. Sutter-Fella[3], David P. Fenning[1,2]

[1]Aiiso Yufeng Li Family Department of Chemical and Nano Engineering, University of California San Diego, 9500 Gilman Drive, La Jolla, California 92093, United States.

[2]Materials Science & Engineering Program, University of California San Diego, 9500 Gilman Drive, La Jolla, California 92093, United States

[3]Molecular Foundry Division, Lawrence Berkeley National Laboratory, 1 Cyclotron Road, Berkeley, California 94710, United States.

[4]Advanced Light Source, Lawrence Berkeley National Laboratory, 1 Cyclotron Road, Berkeley, California 94710, United States.

Materials

Acetone, Isopropanol (IPA), 2-methoxyethanol (2-ME, 99.8%, anhydrous), 1-methyl-2-pyrrolidone (99.5%, anhydrous), Piperazine-1,4-diium iodide (PDI), (3-aminopropyl) triethoxysilane (APTES) (99%), and ethanol (200 proof, anhydrous) were purchased from Sigma Aldrich. PbI_2 (99.99% trace metals basis), Bathocuproine (BCP) and MeO-2PACz (98+%) were purchased from TCI America. C_{60} was purchased from Luminescence Technology Corp. (Lumtec). Formamidinium iodide, and methylammonium chloride (MACl) were purchased from Greatcell. The above chemicals were used as received without further modification. ITO substrates were procured from Biotain Crystal Co. Limited.

Device fabrication

The substrates were cleaned sequentially with deionized (DI) water, acetone, and isopropanol (IPA) for 15 min each, followed by surface activation via UV–ozone (UVO_3) treatment for 20 min. A self-assembled monolayer (SAM) of MeO-2PACz (0.6 mg mL^{-1} in ethanol) was deposited by spin coating at 3000 rpm (acceleration: 500 rpm s^{-1}) for 30 s, and subsequently annealed at 100 °C for 10 min.

The $FAPbI_3$ perovskite precursor was prepared by dissolving 1.33 M PbI_2 and 1.33 M FAI in 2-methoxyethanol (2-ME) under vortex mixing in a 4 mL vial. 15.0 mol% MACl and 2.5% PbI_2 (relative to $FAPbI_3$) were then added as additive.[1] The precursor solution was deposited onto the SAM-coated substrates by spin coating at 8000 rpm (acceleration: 2000 rpm s^{-1}) for 30 s, followed by thermal annealing at 150 °C for 10 min under controlled deposition environments (N_2, RH 0%, RH 10%, and RH 20%). We built an open loop humidity-controlled chamber where dry air and humid air were blended in precise ratios to create the desired environment for perovskite deposition.

Further, the perovskite surface was passivated by spin coating a PDI solution (0.5 mg mL^{-1} in IPA) at 5000 rpm for 20 s, with a subsequent annealing step at 85 °C for 5 min. Finally, C_{60} (30 nm) and BCP (13 nm) layers were deposited via thermal evaporation, followed by the evaporation of a 100 nm Ag top electrode to complete the device architecture.

Characterizations

WAXS measurements were carried out during spin coating 1.33 M $FAPbI_3$ with MACl additive at 4000 rpm (acceleration: 2000 rpm s^{-1}) for 30 s, followed by thermal annealing (both normal and ramped) to track the crystallization pathway. The deposition environment was maintained using a similar humidity controller setup as employed for device fabrication. The incident X-ray beam was aligned at 1° with an energy of 10 keV. Scattering was recorded with a DECTRIS Pilatus 1M detector placed at 35° relative to the sample plane, with a fixed sample-to-detector distance of ~189 mm. The beam footprint on the sample measured 115 µm × 5 µm (575 $µm^2$), with a flux of ~10^9 photons $µm^{-2}$ s^{-1}. Detector calibration was performed using an Al_2O_3 powder standard prior to measurements, and the detector position was kept fixed throughout the experiments. For each sample, diffraction from the bare ITO substrate was also collected for additional re-calibration. Diffraction patterns were acquired at a frame rate of 0.56 s^{-1}. The 2D images were initially processed with custom-built software and further analyzed using the pyFAI and pygix Python packages.[2]

To collect the steady state PL data a home-built photoluminescence set up (with 532 nm laser) was used for excitation of the perovskite films. Ex-situ XRD measurements were performed using an Anton Paar XRDynamic 500. SEM imaging was conducted using lens detection on an FEI Apreo SEM, with beam energy and current fixed at 2 kV and 50 pA with T1 detector (Optiplan Mode), respectively. EQE measurements were performed using a home-built system comprising a xenon

arc lamp coupled to a Newport CS260 monochromator equipped with harmonic filters. The monochromatic light beam was mechanically chopped at 493 Hz and focused onto the device active area. Incident light intensity was calibrated using photodiode power sensors (Thorlabs S120VC and S122C), and system accuracy was verified by measuring the J_{SC}, EQE of a calibrated Si reference cell (Abet Technologies, Model 15150), which agreed within 1% of the certified value. EQE spectra were acquired by sweeping the incident wavelength from 300 to 900 nm, with photocurrent signals collected across a 50 Ω shunt resistor and measured via a lock-in amplifier (Stanford Research Systems SR830).

Photoluminescence Quantum Yield and Implied Current-Voltage Curves

Implied current–voltage (*iJV*) characteristics of passivated perovskite films were derived from injection-dependent PLQY measurements, as described in earlier reports.[3] PLQY measurements were carried out on each sample using a home-built setup comprising an integrating sphere (Newport, Model 819C-SF-4) and following the three-measurement approach.[3] Samples were excited with a continuous-wave diode-pumped solid-state 532 nm laser, operated through a laser diode controller (SRS, Model LD502). One port of the integrating sphere was equipped with a switchable-gain Si photodetector (Thorlabs, PDA100A2) and an automated filter slider (Thorlabs, ELLK6) loaded with a 600 nm long-pass filter (Thorlabs, FELH600, O.D. 6). The laser was modulated at 993 Hz, and the photodetector signal was recorded using a lock-in amplifier (SRS, SR830). Implied voltage (*iV*) values across different illumination conditions were determined using the following expression:

$$iV = V_{lim}(J_{ill}) + \frac{k_B T}{q} ln(PLQY)$$

where k_B is the Boltzmann constant, T is the absolute temperature of the sample (fixed at 300K), q is the elementary charge, and $V_{lim}(J_{ill})$ is the radiative voltage limit as a function of photocurrent. Implied voltage is directly proportional to the quasi-Fermi level splitting (QFLS), a parameter limited by non-radiative recombination, which is quantified through PLQY.

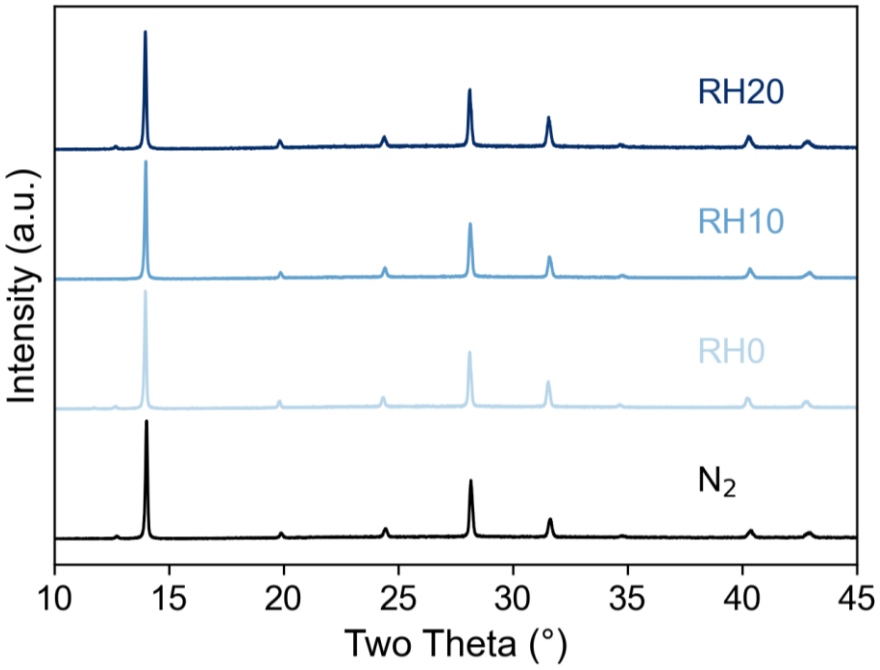

Fig. S1 X-ray diffraction patterns with normal scale for films processed under different environments.

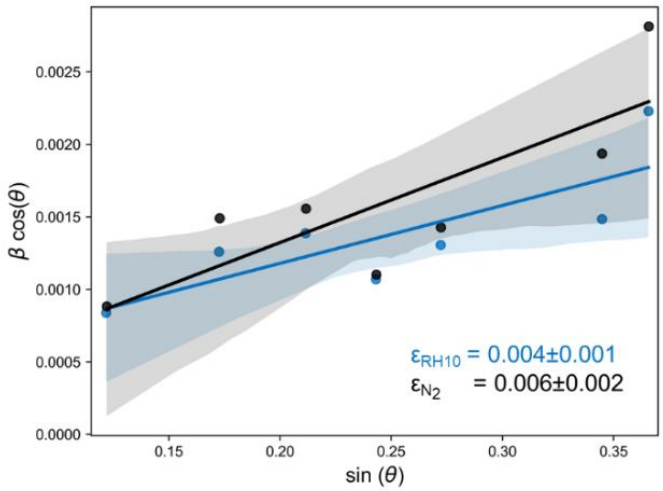

Fig. S2 Williamson-Hall plots of XRD data for microstrain analysis of perovskite films processed under different environments.

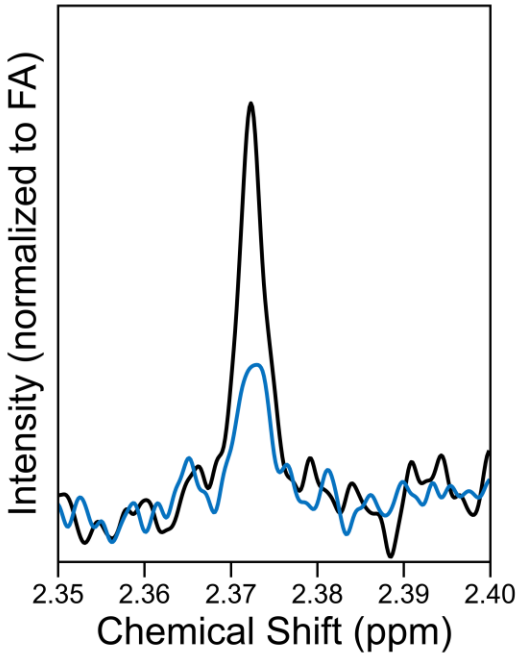

Fig. S3 ^{1}H NMR of perovskite films dissolved in d^{6}-DMSO.

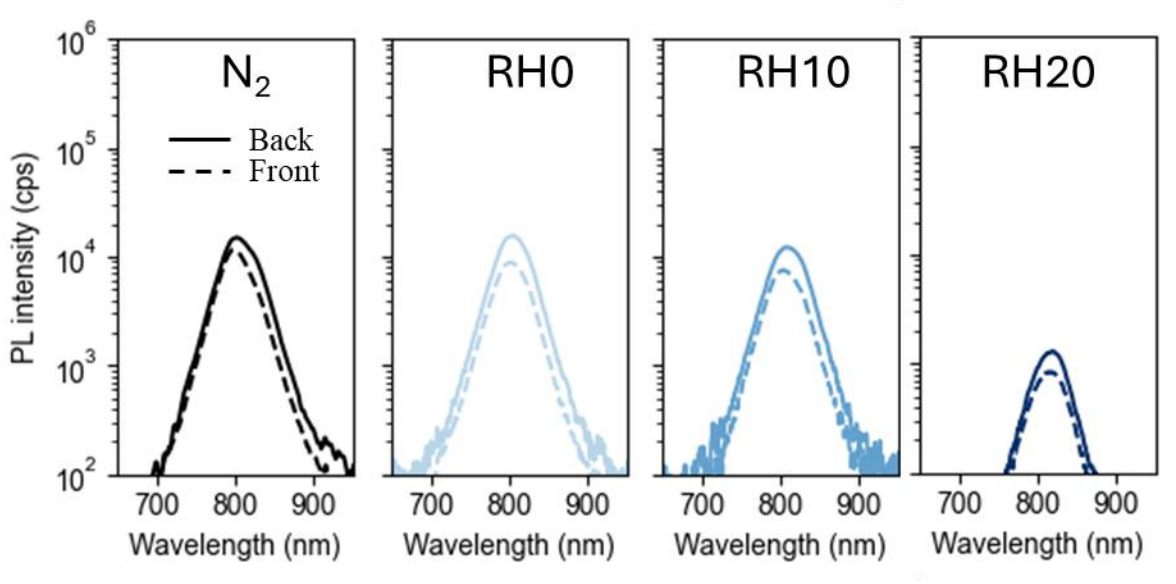

Fig. S4 PL spectra of films processed under different environments (back:glass/perovskite and front:perovskite/air).

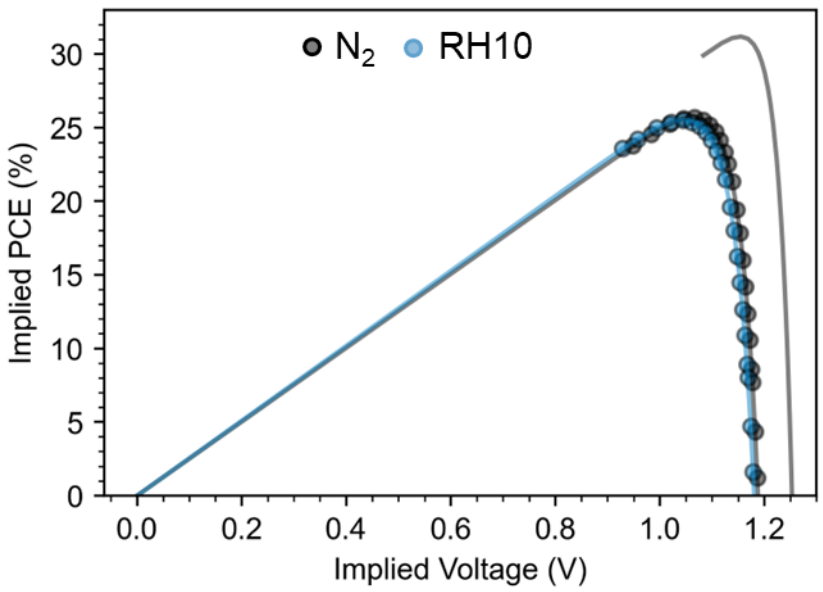

Fig. S5 Implied PCE vs Implied V plot of films processed under N_2 and RH 10% environment.

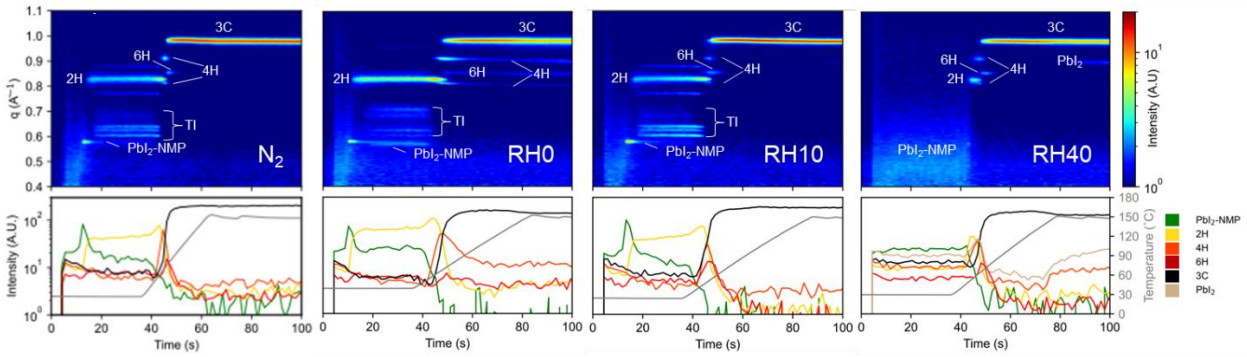

Fig. S6 Heat maps of azimuthally integrated *in situ* WAXS patterns recorded during isothermal annealing of the film under N_2, RH 0%, RH 10%, and RH 40%. The lower panels show the time evolution of selected diffraction peaks extracted from the corresponding datasets.

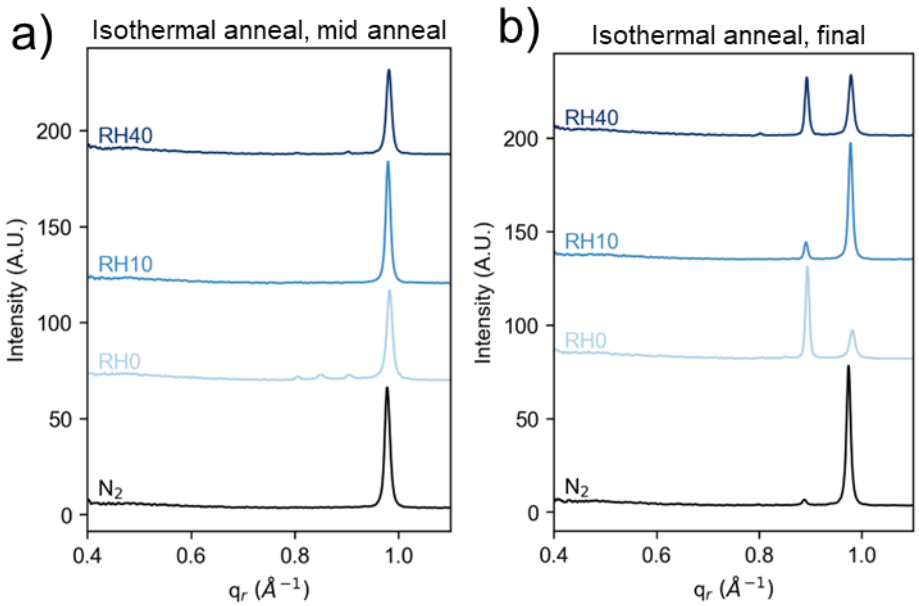

Fig. S7 Integrated WAXS patterns of a) standard isothermal annealed films (mid-annealed) and b) final standard isothermal film processed under different environments. In final films, PbI_2 appeared possibly due to extended annealing.

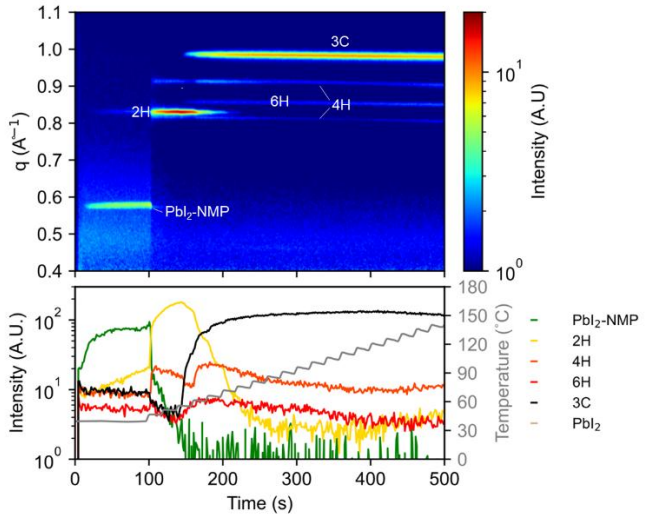

Fig. S8 Heat map of azimuthally integrated *in situ* WAXS of film deposited under RH 40% with ramped annealing.

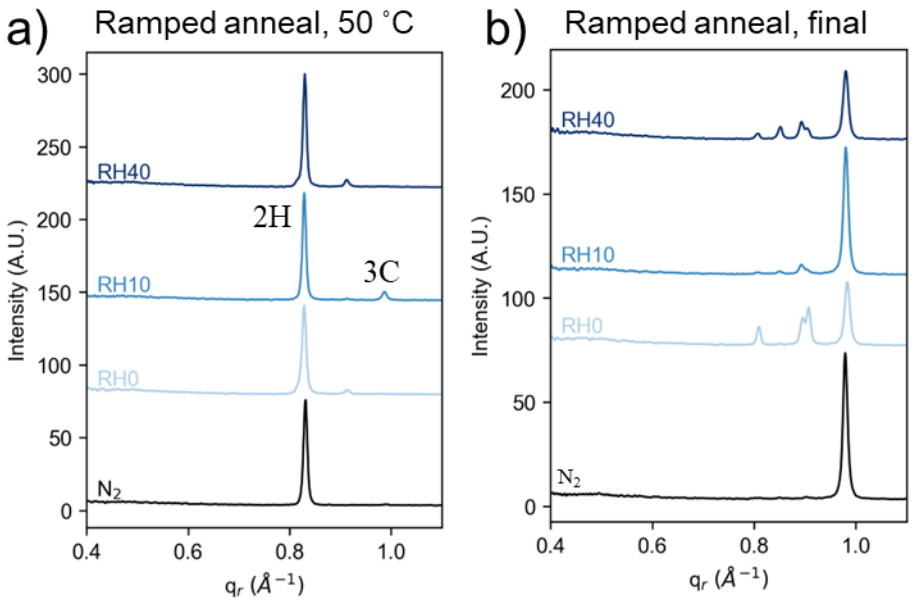

Fig. S9 Integrated GIWAXS patterns of a) films subjected to ramped annealing at 50 °C, and b) final films processed via ramped annealing under different environmental conditions. Prolonged and slow annealing under ambient conditions resulted in some undesired phases in the ambient-processed final films.

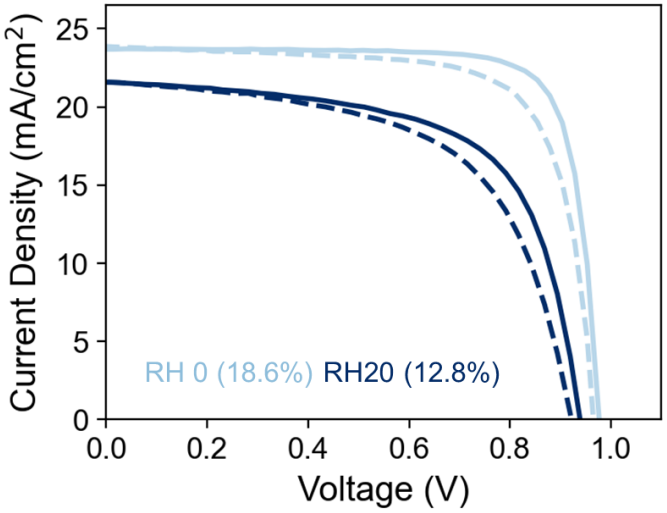

Fig. S10 *J–V* characteristics (dashed = forward scan and solid line = reverse scan) of RH0 and RH20 devices.

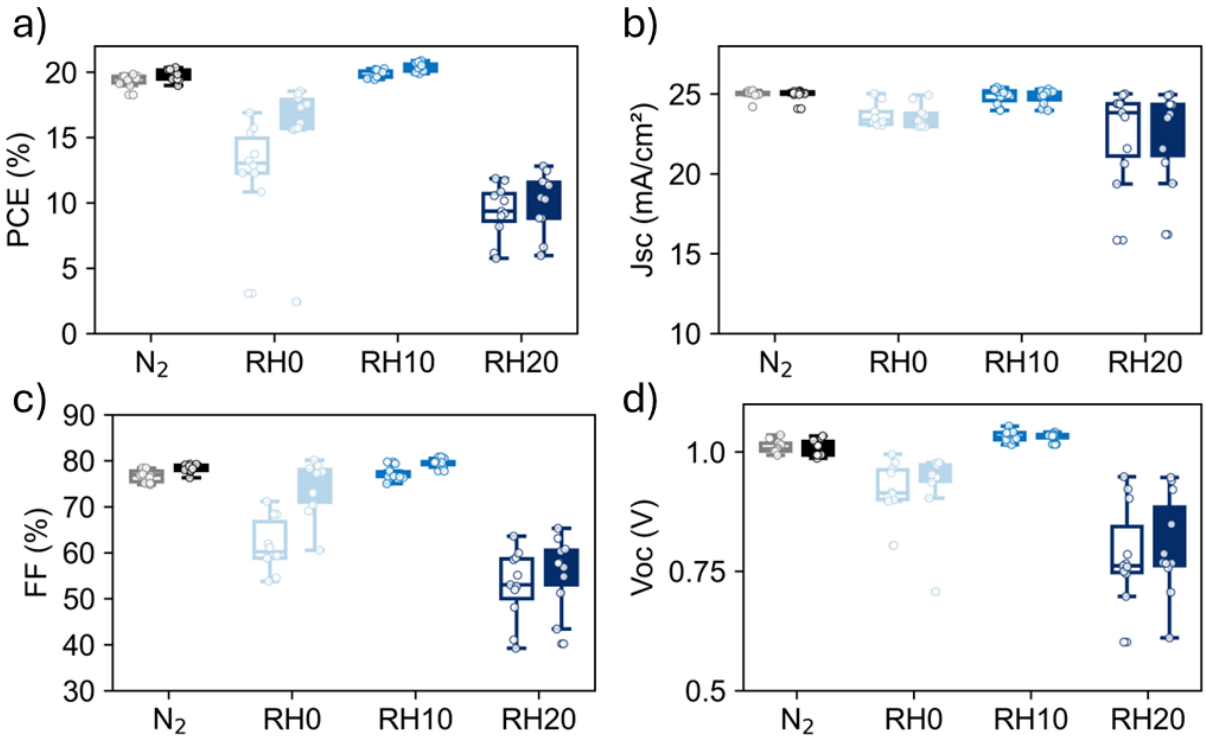

Fig. S11 Box plot of photovoltaic parameters a) PCE, b) J_{SC}, c) *FF*, and d) V_{OC} of 10 devices processed under different conditions.

Table S1. Device data of champion cells

Device	J_{SC}, mA/cm²	*FF*, %	V_{OC}, V	PCE, %
N_2 (REV)	25.0	78.9	1.030	20.40 (19.77±0.44)
N_2 (FWD)	24.9	77.2	1.030	19.85 (19.40±0.48)
RH 10 (REV)	24.9	80.9	1.038	20.95 (20.37±0.33)
RH 10 (FWD)	24.9	78.0	1.040	20.20 (19.84±0.29)

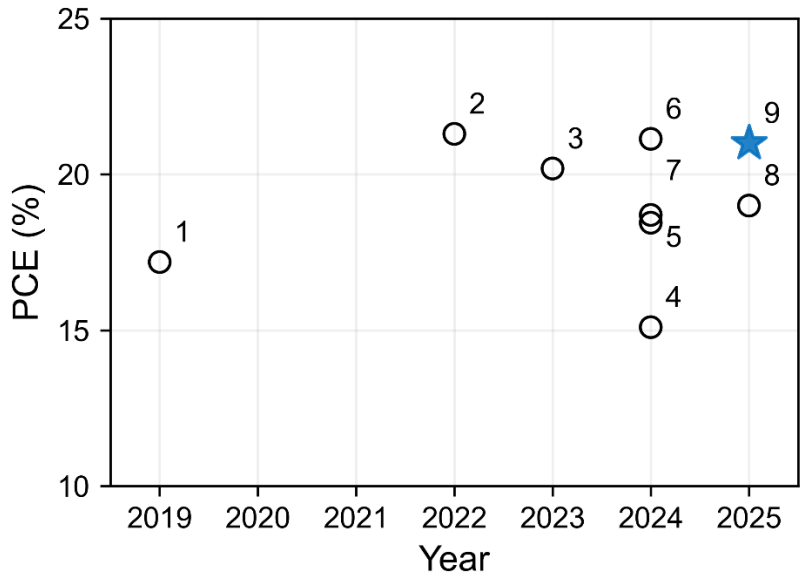

Fig. S12 PCE reported in recent literature on *p-i-n* $FAPbI_3$ device processed under ambient condition (star sign represents this work). References are listed from 4 to 11 respectively. [4–11]

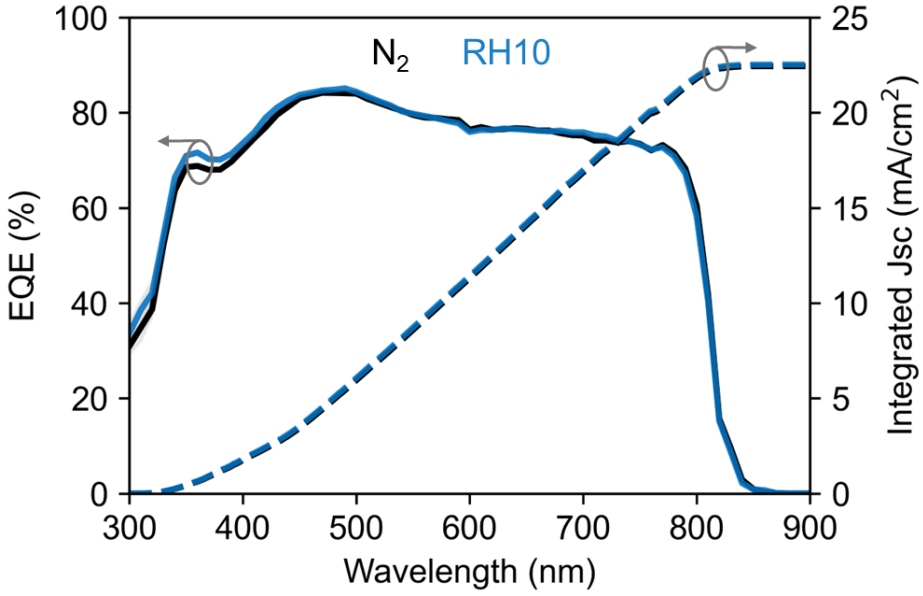

Fig. S13 EQE spectra of devices processed under N_2 and RH10.

References

[1] Q. Zhang, G. Ma, K. A. Green, K. Gollinger, J. Moore, T. Demeritte, P. C. Ray, G. A. Hill, X. Gu, S. E. Morgan, M. Feng, S. Banerjee, Q. Dai, *ACS Appl. Energy Mater.* **2022**, *5*, 1487.

[2] G. Ashiotis, A. Deschildre, Z. Nawaz, J. P. Wright, D. Karkoulis, F. E. Picca, J. Kieffer, *J. Appl. Crystallogr.* **2015**, *48*, 510.
[3] J. R. Palmer, S. Iwamoto, C. Han, C. J. Dolan, H. M. Vossler, S. P. Dunfield, D. P. Fenning, *New J. Chem.* **2025**, *49*, 1223.
[4] G. Wang, L. Wang, J. Qiu, Z. Yan, K. Tai, W. Yu, X. Jiang, *Sol. Energy* **2019**, *187*, 147.
[5] R. Li, J. Ding, X. Mu, Y. Kang, A. Wang, W. Bi, Y. Zhang, J. Cao, Q. Dong, *J. Energy Chem.* **2022**, *71*, 141.
[6] H. Gao, M. Zhang, Z. Xu, Y. Chen, Y. Hu, Z. Yi, J. Huang, H. Zhu, *Dalton Trans.* **2024**, *53*, 136.
[7] N. Vanni, R. Pò, P. Biagini, G. Bravetti, S. Carallo, A. Giuri, A. Rizzo, *Nanomaterials* **2024**, *14*, 107.
[8] L. Cao, Y. Tong, Y. Ke, Y. Chen, Y. Li, H. Wang, K. Wang, *ACS Appl. Mater. Interfaces* **2024**, *16*, 66865.
[9] N. Vanni, A. Giuri, G. Bravetti, R. Marrazzo, E. Quadrivi, C. Marchini, S. Spera, M. R. Guascito, R. Pò, P. Biagini, A. Rizzo, *ACS Appl. Mater. Interfaces* **2024**, *16*, 40927.
[10] N. Vanni, A. Giuri, M. Calora, E. Podda, A. P. Caricato, K. Sparnacci, R. Suhonen, M. Ylikunnari, A. Covarelli, L. Gregori, F. De Angelis, G. Marra, P. Biagini, R. Po, A. Rizzo, *Sol. RRL* **2024**, *8*, 2400612.
[11] N. Vanni, M. Calora, L. Mercurio, A. Giuri, A. P. Caricato, V. Chierchia, C. Carati, R. Po', P. Biagini, S. Valastro, E. Smecca, G. Mannino, A. Alberti, A. Rizzo, *Adv. Sci.* **2025**, *12*, 2501533.